Rhizosphere priming is tightly associated with root-driven aggregate turnover

Xiaohong Wang [a,b,1], Liming Yin [a,1], Feike A. Dijkstra [c], Jiayu Lu [a], Peng Wang [a,*], Weixin Cheng [d]

[a] *CAS Key Laboratory of Forest Ecology and Management, Institute of Applied Ecology, Shenyang, 110016, China*
[b] *University of Chinese Academy of Sciences, Beijing, 100049, China*
[c] *Sydney Institute of Agriculture, School of Life and Environmental Sciences, University of Sydney, Sydney NSW, 2006, Australia*
[d] *Environmental Studies Department, University of California, Santa Cruz, CA, 95064, USA*

ARTICLE INFO

ABSTRACT

The root-driven soil aggregate turnover dynamics and rhizosphere priming effect (RPE, changes in soil organic carbon (SOC) decomposition caused by living roots) are central to the understanding of SOC cycling. However, the association between aggregate turnover and the RPE has not been illuminated in plant-soil systems because of methodological difficulties. Using rare earth oxides to trace the transformations among different aggregates and ^{13}C natural abundance labeling, we for the first time simultaneously investigated aggregate turnover and the RPE at two phenological stages of two grass species (*Agropyron cristatum* and *Koeleria cristata*): tillering (40 days after planting, DAP40) and jointing-heading (DAP63). We found that aggregate turnover rates varied widely, with a range between 0.006 day^{-1} and 0.024 day^{-1}, *i.e.*, turnover times (the reciprocal of turnover rates) ranged from 41 to 168 days, and were significantly influenced by plant species, sampling date and their interaction. Particularly, greater aggregate turnover rates (2% ~ 68%) and transformations in breakdown and formation pathways were found for *K. cristata* than for *A. cristatum* at DAP63. The RPEs increased with plant growth and ranged from −29% to +163%. Especially, the RPE and microbial biomass C were significantly greater for *K. cristata* than for *A. cristatum* at DAP63. Root-driven aggregate turnover was tightly associated with the RPE, possibly because of the release of aggregate-protected C for microbial decomposition. There was no net C loss mainly because increased aggregate formation could have sequestrated root-derived C in macroagrgegates and thus counteracted the C loss by the positive RPE. We therefore propose a new framework of root-driven aggregate turnover for considering how plant roots influence SOC dynamics via aggregate turnover. Root-accelerated aggregate turnover acts as a "key": enhancing SOC decomposition (*i.e.* RPE), while simultaneously accelerating the occlusion of root-derived C and thus facilitating new C sequestration. This framework highlights that living root-driven aggregate turnover alters the physical protection of SOC and regulates the RPE, which aligns well with the emerging perspective of SOC stabilization.

1. Introduction

Globally, soil organic carbon (SOC) decomposition releases CO_2 as much as 7 times of the CO_2 flux from fossil fuel burning and land-use change and plays a critical role in the global C cycle and soil-climate feedback (Bond-Lamberty and Thomson, 2010; Lehmann and Kleber, 2015). Together with factors such as mineral adsorption and biomolecular recalcitrance, physical protection of SOC relating to soil aggregate dynamics is an important factor controlling SOC decomposition (Lützow et al., 2006; Lehmann and Kleber, 2015). Emerging evidence suggests that physical protection provided by soil aggregates could be a pivotal ecosystem property for SOC persistence (Schmidt et al., 2011). However, our understanding of the root-driven aggregate turnover and subsequent effects on SOC decomposition is limited.

Soil aggregate turnover involves aggregate formation and breakdown processes (Plante and McGill, 2002; Six et al., 2004). Indeed,

---

compared to the extent of soil aggregation, aggregate turnover could play a predominant role in determining SOC dynamics, particularly decomposition (Six et al., 2004; De Gryze et al., 2006). However, the direct empirical evidence of the association between aggregate turnover and SOC decomposition is insufficient thus far (Plante and McGill, 2002; Six et al., 2004; Stamati et al., 2013). Previous studies only indirectly determined aggregate turnover by investigating either net changes in aggregation (Yoo and Wander, 2008; Bach and Hofmockel, 2016), or the accumulation or loss of organic matter in aggregates with time (Six et al., 2001; Chivenge et al., 2011; Gentile et al., 2011). These studies did not separate aggregate formation from breakdown processes (Plante and McGill, 2002). However, a few recent laboratory studies documented that rare earth oxides (REOs) can be used to trace all the transformation processes among aggregates, and thus to quantify their turnover rates (e. g., De Gryze et al., 2006; Peng et al., 2017; Rahman et al., 2019).

Living roots are considered to be one of the most important drivers of aggregate turnover (Six et al., 2004). For example, some studies observed an increase in soil aggregation by the presence of roots (Haynes and Beare, 1997; Blankinship et al., 2016; Gould et al., 2016), i.e., a larger increase in aggregate formation compared to aggregate breakdown, depending on plant species or growth stage (Poirier et al., 2018a). Meanwhile, root-derived C could be occluded within the newly formed aggregates, particularly in macroaggregates (Anger et al., 1997; Gale et al., 2000). These results indicate that living roots may have greater influences on aggregate formation than breakdown processes, and highlight their differential effects on altering turnover rates of aggregates with different sizes. However, the extent to which turnover rates of aggregates of different sizes are influenced by living roots is still poorly understood, which may further impede our prediction of how SOC is affected by root-driven aggregate turnover.

The effect of living roots on SOC decomposition has been termed the rhizosphere priming effect (RPE), which is defined as the stimulation or suppression of SOC decomposition by live roots and associated rhizosphere organisms when compared to SOC decomposition from rootless soils under the same environmental conditions (Kuzyakov, 2002). The RPE is of great importance in regulating SOC decomposition (Cheng et al., 2014; Finzi et al., 2015; Huo et al., 2017). The RPE ranges widely, from −50% (a retardation) to +380% (a stimulation) compared to rootless soil (Cheng et al., 2014). Several experimental lines of evidence have shown that the RPE could be attributed to microbial growth and activity (e.g., Zhu et al., 2014; Yin et al., 2019), and plant species (e.g., Yin et al., 2018) and associated attributes such as biomass (Huo et al., 2017) and fine root morphology (Pausch et al., 2016). On the other hand, the extent of soil C accessibility associated with physical and chemical protection can also significantly influence the magnitude of the RPE (e.g., Keiluweit et al., 2015; Lu et al., 2019; Wang et al., 2020). However, to our best knowledge, no studies have investigated the role of root-driven aggregate turnover in regulating the RPE yet.

According to the aggregate turnover hypothesis (Cheng and Kuzyakov, 2005; Cheng et al., 2014), accelerated aggregate turnover (especially aggregate breakdown) may release SOC that was previously inaccessible because of occlusion within aggregates and thus may intensify the positive RPE, and meanwhile may occlude root-derived C into newly formed aggregates, which could to some extent counteract the RPE-induced SOC loss (Cheng et al., 2014). This exploratory hypothesis is important as it aligns well with the emerging perspective that the stabilization of SOC is controlled by physicochemical protection and microbial accessibility (Schmidt et al., 2011). However, this critical hypothesis has not been validated by empirical evidence (Cheng et al., 2014). Notably, simultaneous quantification of aggregate turnover and the RPE is needed to fill this key knowledge gap, i.e., the extent to which both SOC formation and decomposition are accounted for by soil aggregate turnover.

Here we conducted an experiment by employing a ^{13}C natural abundance approach combined with a REO tracer method. We grew two C$_3$ grasses in a soil that was reconstructed from four aggregate fractions labeled with different REOs, which all came from the same C$_4$ soil. Thus, we were able to simultaneously quantify the transformation rates among aggregate fractions (Fig. S1) and the RPE. We hypothesized that (1) planting would increase aggregate turnover rates, which would vary with plant growth (i.e. time), with an increase in net soil aggregation (i. e., formation higher than breakdown) (Poirier et al., 2018a), and (2) differences in the RPEs would be especially positively associated with the enhanced aggregate turnover rates (especially breakdown) across species, and at the same time aggregate formation would lead to increased incorporation and protection of root-derived C in the newly formed aggregates (Cheng and Kuzyakov, 2005; Cheng et al., 2014).

2. Materials and methods

2.1. Soil material

In this study, a C$_4$ soil was used with a ^{13}C natural tracer approach to separate soil-derived CO$_2$–C (C$_4$–C) from root-derived CO$_2$–C (C$_3$–C). The C$_4$ soil was taken from the plow layer (0–20 cm depth) of a continuous maize field (>23 years), air-dried, passed through a 4 mm sieve and homogenized. The soil is classified as a Mollisol derived from the sedimentary materials of loamy loess. It contained 1.84% C, 0.16% N, 43% sand, 22% silt and 35% clay, and had a pH of 6.8, and a δ^{13}C value of −20.4‰. Based on a wet-sieving method (see below), the soil comprised of large macroaggregates (>1 mm, LMA), small macroaggregates (0.25–1 mm, SMA), microaggregates (0.053–0.25 mm, MA), and silt & clay fraction (<0.053 mm, SCF), with the corresponding proportions of 10.5%, 29.9%, 44.6% and 15.0%, respectively. The background values of the four REOs in the soil we used were 27.2 mg kg^{-1} Lanthanum oxide (La$_2$O$_3$), 2.01 mg kg^{-1} Samarium oxide (Sm$_2$O$_3$), 24.7 mg kg^{-1} Neodymium oxide (Nd$_2$O$_3$) and 9.74 mg kg^{-1} Gadolinium oxide (Gd$_2$O$_3$).

2.2. Experimental setup

The treatments of this experiment included two plant species (*Agropyron cristatum* (Linn.) Gaertn and *Koeleria cristata* (Linn.) Pers.) and an unplanted control. We chose these two grass species because they are dominant and common species in grasslands of Inner Mongolia, China (Yang et al., 2019), while their impacts on biogeochemical processes have been less investigated compared to other grasses likely *Leymus chinnensis* and *Medicago sativa* (Lu et al., 2019). We performed two destructive samplings at 40 and 63 days after planting (DAP40 and DAP63) corresponding to the tillering and jointing-heading stages, respectively. Four replicates for the unplanted control, and 5 replicates for each planted treatment were kept at each sampling date with a total of 28 pots. Before planting, we firstly labeled four different aggregate fractions with different REOs and then reassembled these four fractions into a "REOs labeled" soil (see *REOs labeling*). In order to evaluate the potential effect of REOs on SOC decomposition, microbial growth and aggregate distribution, we also included a blank treatment without REOs addition (4 replicates) and found that there was no significant difference between the blank treatment and the unplanted control with REOs labeled at both sampling dates (Table S1). Three extra pots of each species were maintained to measure isotopic fractionation between root tissue and root-derived CO$_2$ (see *Calculations*).

We packed 200 g air-dried "REOs labeled" soil (see below) into each polyvinyl chloride (PVC) pot (height 15 cm, diameter 5 cm, with a sandbag containing 50 g quartz sand at the bottom), equipped with an inlet tube at the bottom and an outlet tube on the side-wall near the top (below soil surface) of each pot for aeration and CO$_2$ trapping. Nutrient solution (NH$_4$NO$_3$) was applied to soils of all pots (including unplanted pots) which amounted to 300 kg N ha^{-1} surface area equivalent. Soil moisture was kept at 60% water holding capacity (WHC) by gently watering with a sprayer. Then we planted ten pots for each species and sowed five seeds on the surface (about 0.5 cm depth) in each pot. After

germinating, two seedlings remained per pot. Anaerobic conditions of all pots were prevented by forcing ambient air into the soil for 5 min every 3 h with an aquarium air pump and a digital timer.

2.3. REOs labeling

We labeled each of the four soil aggregate fractions with a distinctive REO tracer (Peng et al., 2017). Briefly, we first split the soil into five batches, four of which were mixed with one of the four REOs with the remaining one as a blank. REO tracers were sprayed as suspensions with a concentration of 600 mg REO kg^{-1} soil, while continuously mixing the soil to homogenize labeling. After equilibrating for one week and oven-drying at 50 °C for two days, soils were separated into four aggregate fractions, *i.e.*, large macroaggregates, small macroaggregates, microaggregates and silt & clay fraction. The homogeneity of labeling was checked by sampling 3 replicates of each aggregate fraction and measuring the recovery of labeled REO on an ICP-MS (see below). Subsequently, we selected four aggregate fractions containing different REOs to recombine an "REO labeled" soil, where aggregate size distribution (proportion of each fraction expressed as % of total soil weight) was kept unchanged. The blank treatment was subjected to the same procedure except for addition of REOs.

2.4. Soil CO$_2$ trapping

We measured soil respiration of each pot at DAP40 and DAP63 by a CO$_2$ trapping method (Keith et al., 2015). Briefly, we sealed each pot with non-toxic silicone rubber on the surface of the soil. After testing for air leakage, a soda lime column, a pump, and a needle valve were connected to the tube at the bottom of each pot in sequence to remove the initial CO$_2$ inside for 1 h. Then CO$_2$ subsequently produced in each pot during a 48-h period was trapped by connecting a plastic bottle containing 22 mL 0.5 M NaOH solution, and a one-way valve to the tube on the top of the bottle. During CO$_2$ trapping, each pot was ventilated with CO$_2$-free air at a constant flow rate of 90–100 mL min^{-1} controlled by a needle valve for 15 min every 3 h with a digital timer.

During the second CO$_2$ trapping, we investigated the ^{13}C isotopic fractionation between root respiration and root tissue using three extra pots (Wang et al., 2016). Plants were transferred into pots with 250 g acid-washed glass beads (0.25–0.3 mm) after washing roots carefully. We then collected root respiration using the same CO$_2$ trapping method as mentioned above. An aliquot of each NaOH solution was analyzed for total inorganic C using a multi N/C® 2000 TOC analyzer (Analytik Jena, Germany). Another aliquot was analyzed for δ^{13}C using cavity ring-down spectroscopy (CRDS) with Automate Module (Picarro G2131-i Analyzer, Picarro Inc., Santa Clara, CA, USA).

2.5. Harvesting and measurements

After CO$_2$ trapping, plant shoots were cut off at the soil surface. In order to minimize the potential effect of harvesting on aggregates, the soil was slipped out of pots by gently beating the pots. After roots were collected carefully with tweezers, the fresh soil was immediately passed through a 4 mm sieve by gently breaking apart the soil to measure soil moisture, microbial biomass carbon (MBC), aggregate size distribution and REO concentrations. Cleaned fine roots (at DAP63) were scanned with a Microtek ScanMaker (MICROTEK, China) and analyzed with a root analysis system (Wseen, China) to determine specific root length, specific surface area, root length density, mean diameter, and the percentage of root length with different diameters (<0.5 mm and 0.5–2 mm). Shoots and roots were oven-dried at 60 °C for 48 h, weighed, and ground by a ball mill for δ^{13}C and C concentration analyses.

The MBC was measured by the chloroform fumigation-extraction method (Vance et al., 1987). Briefly, 10 g fresh soil was fumigated with non-ethanol chloroform for 24 h, then fumigated and non-fumigated subsamples were extracted with 40 mL 0.05 M K$_2$SO$_4$

solution. The extracts were measured for total organic C (TOC) using a multi N/C® 2000 TOC analyzer. MBC was calculated as the difference in TOC between fumigated and non-fumigated extracts with a conversion factor of 0.45.

Water-stable aggregates were separated by a wet-sieving method (Elliott, 1986). Briefly, a 60 g air-dried subsample was placed on the top of a stack of sieves (1 mm, 0.25 mm and 0.053 mm) and submerged in water for 5 min. Then we manually moved the sieves up and down for 50 repetitions in 2 min. Stable aggregates remaining on these sieves were oven-dried at 50 °C and weighed, representing the large macroaggregates, small macroaggregates, and microaggregates, respectively. Fractions lower than 0.053 mm were collected, centrifuged and oven-dried at 50 °C, representing the silt & clay fraction. All aggregates were ground for REOs, δ^{13}C and C concentration analyses.

REOs of each aggregate fraction were extracted by digestion (Zhang et al., 2001; De Gryze et al., 2006). Briefly, 0.100 g of fine powder was weighed into a 30 mL Teflon crucible, with 2 mL HNO$_3$ (70%), 2 mL H$_2$O$_2$ (30%, removing organically-bound REOs) and 1 mL HCl (36%), and placed with a cover overnight. Samples were then heated at 95 °C for 3 h in a water bath. After cooling, samples were washed, filtered (0.45 μm), centrifuged, and analyzed using an ICP-MS for REO concentration (NexION 300X, PerkinElmer, USA).

C concentration and δ^{13}C of subsamples for plant biomass, bulk soil and aggregate fractions were analyzed on an elemental analyzer (vario MACRO cube, Elementar, Germany) and on CRDS with Combustion Module (Picarro G2131-I Analyzer, Picarro Inc., Santa Clara, CA, USA), respectively.

2.6. Calculations

The turnover rate, REO recovery, and mean weight diameter (MWD) for each aggregate fraction were calculated by following the method in Peng et al. (2017). Taking the turnover rate of large macroaggregate (T$_{rate}$ (LMA)) for example, the calculation was as follows:

$$T_{rate} (LMA) = (a + d + f)/t \tag{1}$$

where *a*, *d* and *f* are the transformations (% of the initial amount of each aggregate fraction) out of large macroaggregates (Fig. S1) at DAP40 or at DAP63; and *t* is the corresponding time interval from DAP0 to DAP40 or to DAP63 (*i.e.*, 40 days and 63 days, respectively). For details please see the supplementary material.

The recovery of REOs for La$_2$O$_3$, Sm$_2$O$_3$, Nd$_2$O$_3$, and Gd$_2$O$_3$ ranged between 98% and 101% after initially labeling, and between 90% and 102% for the two sampling dates, which was comparable to that reported by Peng et al. (2017). In order to test for the efficacy of REOs for tracking aggregates transformation, we compared the predicted MWD with the measured MWD (De Gryze et al., 2006). The regression between the predicted MWD and the measured MWD was very close to the 1:1 line ($R^2 = 0.975$, $P < 0.001$; Fig. S2), indicating that the REO labeling method was robust and effective in tracing aggregate turnover.

We separated soil-derived CO$_2$ (C$_{soil}$, mg C kg^{-1} soil d^{-1}) from root-derived CO$_2$ (C$_{root}$, mg C kg^{-1} soil d^{-1}) in the planted treatments using a two-source mixing model (Cheng et al., 2003). Then, the RPE (%) was calculated as the difference in soil-derived CO$_2$ between the planted and unplanted treatments:

$$RPE = \left[C_{soil(planted)} - C_{soil(unplanted)} \right] / C_{soil(unplanted)} \times 100 \tag{2}$$

During the above calculations, we accounted for the magnitude of ^{13}C isotopic fractionation for root-derived CO$_2$, which was -1.46 ± 0.18‰ and -1.93 ± 0.19‰ for *A. cristatum* and *K. cristata*, respectively.

2.7. Statistics

Two-way ANOVA was used to assess the effects of planting, sampling date and their interaction on soil-derived CO$_2$, MBC, MWD, C
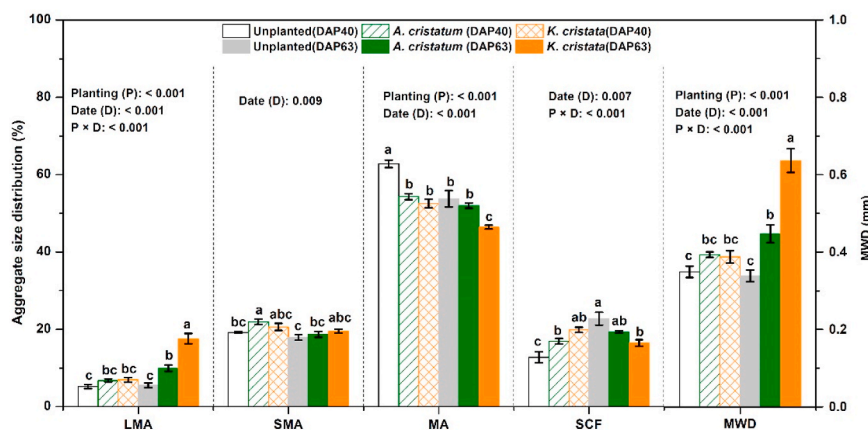
Fig. 1. Size distribution of the four aggregate fractions and mean weight diameter (MWD). LMA, SMA, MA and SCF indicate the large macroaggregates, small macro-aggregates, microaggregates and silt & clay fraction, respectively, and are expressed as a percentage of the total soil weight. Different lowercase letters indicate significant differences in the same aggregate fraction among treatments across the two sampling dates. Sub-legend shows ANOVA *P*-values. Date represents the sampling date. Error bars indicate standard errors of the mean; n = 4 for unplanted control and n = 5 for planted treatments except for the *A. cristatum* treatment at the second sampling date, where n = 3.

concentration and $\delta^{13}C$ value in bulk soil and aggregate fractions, aggregate distribution and turnover rates, and all the transformations (breakdown and formation pathways) among aggregate fractions. Two-way ANOVA was also used to examine the effects of species, sampling date and their interaction on the RPE, plant biomass and root-derived CO_2. *Post hoc* Tukey's test was used to compare differences among means. Two-tailed *t*-test was used to assess differences in fine root traits between species, and differences in soil-derived CO_2, MBC, MWD and aggregate distribution between the blank soil (without REOs addition) and the unplanted control soil (with REOs addition). One-tailed *t*-test

was used to determine if root-derived C in the large macroaggregates was larger than zero, and if the transformations from DAP40 to DAP63 were significantly different from zero. Simple linear regression was used to assess the relationship between measured and predicted MWD. As the biomass of *A. cristatum* in two pots was abnormally low compared to the other three pots at DAP63, we removed these from the analyses. All statistical analyses were performed with SPSS 21 and the significance level was set at *P* < 0.05.
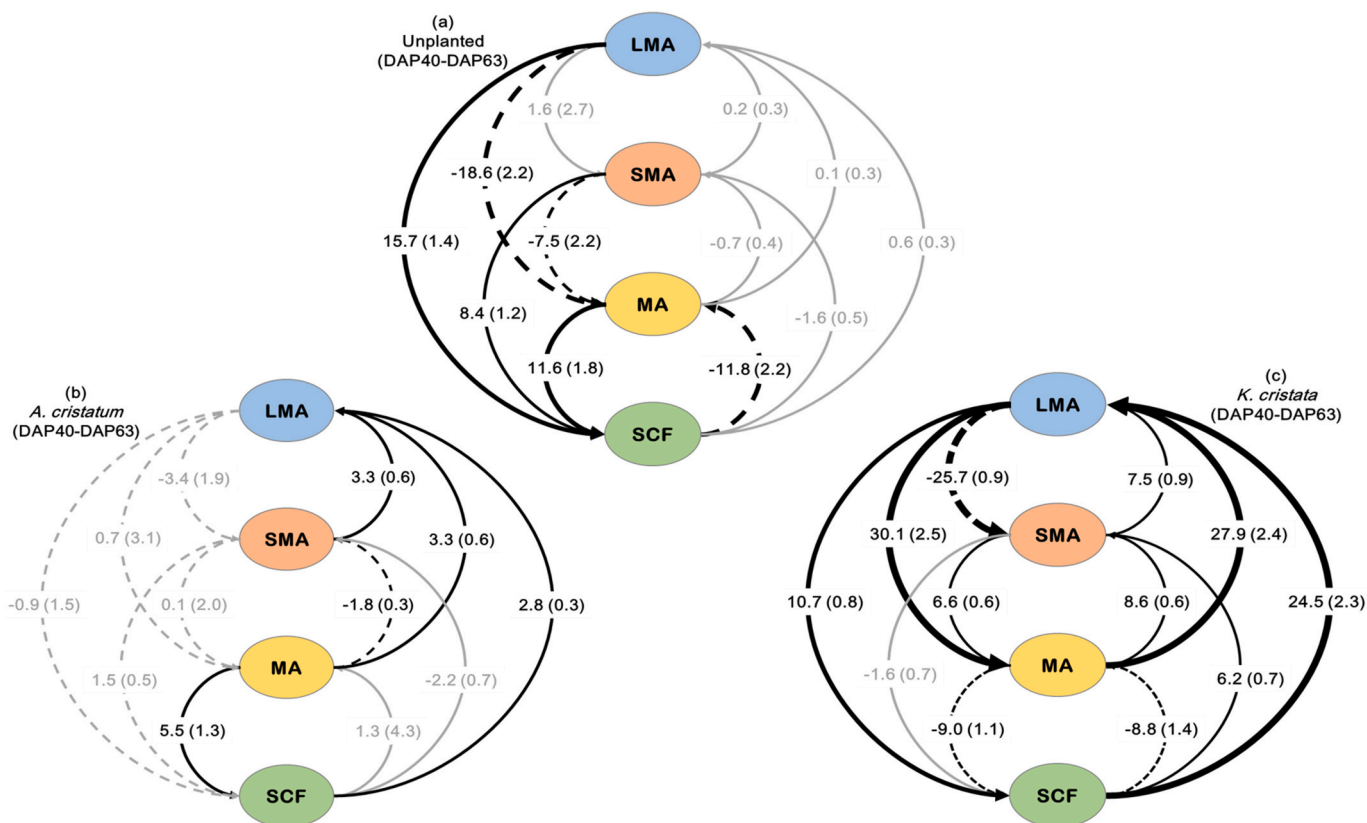
Fig. 2. Transformations between the four aggregate fractions from DAP40 to DAP63 in the unplanted control (a), A. *cristatum* (b) and K. *cristata* (c) treatments, respectively. LMA, SMA, MA and SCF indicate the large macroaggregates, small macroaggregates, microaggregates and silt & clay fraction, respectively. Grey, solid and dashed black arrows indicate that the transformations were without significant difference from zero, significantly higher and significantly lower than zero, respectively (one-tailed *t*-test, *P* < 0.05), while values for each pathway indicate the percent change from DAP40 to DAP63. Thicker arrows indicate greater transformations. n = 4 for unplanted control and n = 5 for planted treatments except for the *A. cristatum* treatment at the second sampling date, where n = 3.
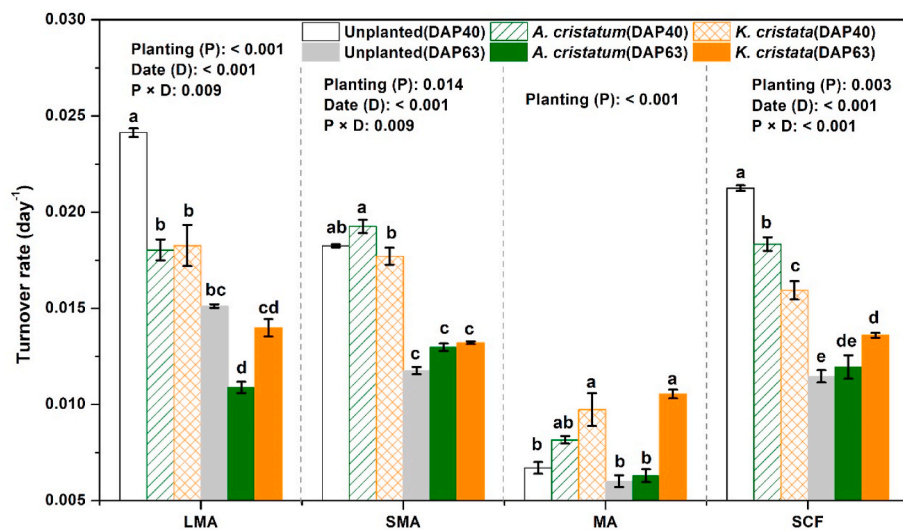
Fig. 3. Turnover rate of the four aggregate fractions. LMA, SMA, MA and SCF indicate the large macroaggregates, small macroaggregates, microaggregates and silt & clay fraction, respectively. Different lowercase letters indicate significant differences among treatments across the two sampling dates. Sub-legend shows ANOVA *P*-values. Date represents the sampling date. Error bars indicate the standard error of the mean; n = 4 for unplanted control and n = 5 for planted treatments except for the *A. cristatum* treatment at the second sampling date, where n = 3.

3. Results

3.1. Aggregate size distribution and MWD

Planting, and its interaction with sampling date significantly influenced the distribution of all aggregates, except for small macroaggregates (*P* < 0.001; Fig. 1). Compared to the unplanted control, planting significantly increased large macroaggregates on average by 148% at DAP63 (planting × sampling date; *P* < 0.001), but decreased microaggregates on average by 14% at both sampling dates (Fig. 1). Silt & clay fraction initially increased and then decreased by planting (Fig. 1). Sampling date had significant influences on the distribution of all aggregates (*P* < 0.01; Fig. 1). With time, large macroaggregates increased on average by 69%, and although other aggregates significantly decreased, the MWD increased (Fig. 1). Furthermore, compared to the unplanted control, the MWD was significantly enhanced by planting, with a 48% increase at DAP63 than at DAP40 (planting × sampling date; *P* < 0.001; Fig. 1).

3.2. Aggregate turnover

Across both sampling dates, planting significantly increased all the formation pathways (*P* < 0.05; Table S2), especially the formation from small macroaggregates, microaggregates and silt & clay fraction to large macroaggregates on average by 175%, 336% and 318%, respectively, compared to the unplanted control (Fig. S3). For the breakdown pathways, averaged across species and sampling date, planting significantly decreased the breakdown from large macroaggregates to microaggregates and silt & clay fraction by 39% and 29%, and increased the breakdown from large macroaggregates to small macroaggregates by 146% (*P* < 0.05; Fig. S3; Table S2). Many transformations changed with time (significant sampling date effects; Fig. S3; Table S2), however, the direction and magnitude of time changes were dependent on planting, resulting in sampling date × planting interactions (*P* < 0.05; Fig. S3; Table S2). With time, the breakdown pathways from larger aggregates to silt & clay fraction significantly increased, and the breakdown pathways from large- and small macroaggregates to microaggregates significantly decreased in the unplanted control (Fig. S3). In contrast, planting significantly increased the breakdown pathways from large- and small macroaggregates to microaggregates, and the formation pathways to large- and small macroaggregates (Fig. S3).

The transformations between aggregate fractions from DAP40 to DAP63 were dependent on species (Fig. 2). For *A. cristatum*, only the transformations in the breakdown pathway from microaggregates to silt & clay fraction and the formation pathways to large macroaggregates were significant, but did not exceed 6% (*P* < 0.05; Fig. 2b). However, for *K. cristata*, all the transformations in the breakdown and formation pathways were significant except for the breakdown from small macroaggregates to silt & clay fraction (*P* < 0.05; Fig. 2c). Especially, the transformations in the breakdown pathway from large macroaggregates to microaggregates and in the formation pathways from microaggregates (and silt & clay fraction) to large macroaggregates were large, around 30% (*P* < 0.05; Fig. 2c).

There were significant effects of planting, sampling date and their interaction on the turnover rates of the four aggregate fractions (*P* < 0.05; Fig. 3). Planting significantly accelerated the turnover rate of microaggregates, particularly for *K. cristata* at DAP63 where the turnover rate was accelerated by 75% in comparison to the unplanted control (*P* < 0.05; Fig. 3). By contrast, planting significantly reduced the turnover rate of large macroaggregates, particularly for *A. cristatum* at DAP63 where the turnover rate was reduced by 28% (*P* < 0.05; Fig. 3). At DAP63, the turnover rates of large macroaggregates, microaggregates and silt & clay fraction were higher for *K. cristata* than for *A. cristatum* by 29%, 68% and 14%, respectively (Fig. 3).

3.3. Soil-derived CO_2, RPE, MBC, plant biomass, root-derived CO_2 and root traits

Compared to the unplanted control, planting significantly enhanced soil-derived CO_2 on average by 119% at DAP63, particularly for *K. cristata* (planting × sampling date; *P* < 0.05; Fig. 4a), but had no significant influence at DAP40. The RPE varied largely with a range from −29% to +163% (Fig. 4b). At DAP63, the RPE caused by *K. cristata* was 120% higher than *A. cristatum* (*P* < 0.05; Fig. 4b). Similarly, planting significantly increased MBC on average by 121% (*P* < 0.05; Fig. 4c), especially for *K. cristata* at DAP63 (planting × sampling date; *P* < 0.05; Fig. 4c).

Plant biomass and root-derived CO_2 significantly increased with time (*P* < 0.001), and were greater for *K. cristata* than *A. cristatum* especially at DAP40 (except for root biomass; *P* < 0.05; Fig. S4). Root traits (except for N concentration and C:N ratio) differed between the two species (Table S3). Especially, *K. cristata* had significantly higher C concentration, specific root length, root length density, and fraction of root length (relative to total length) in the 0–0.5 mm diameter size class than *A. cristatum* (*P* < 0.05; Table S3).
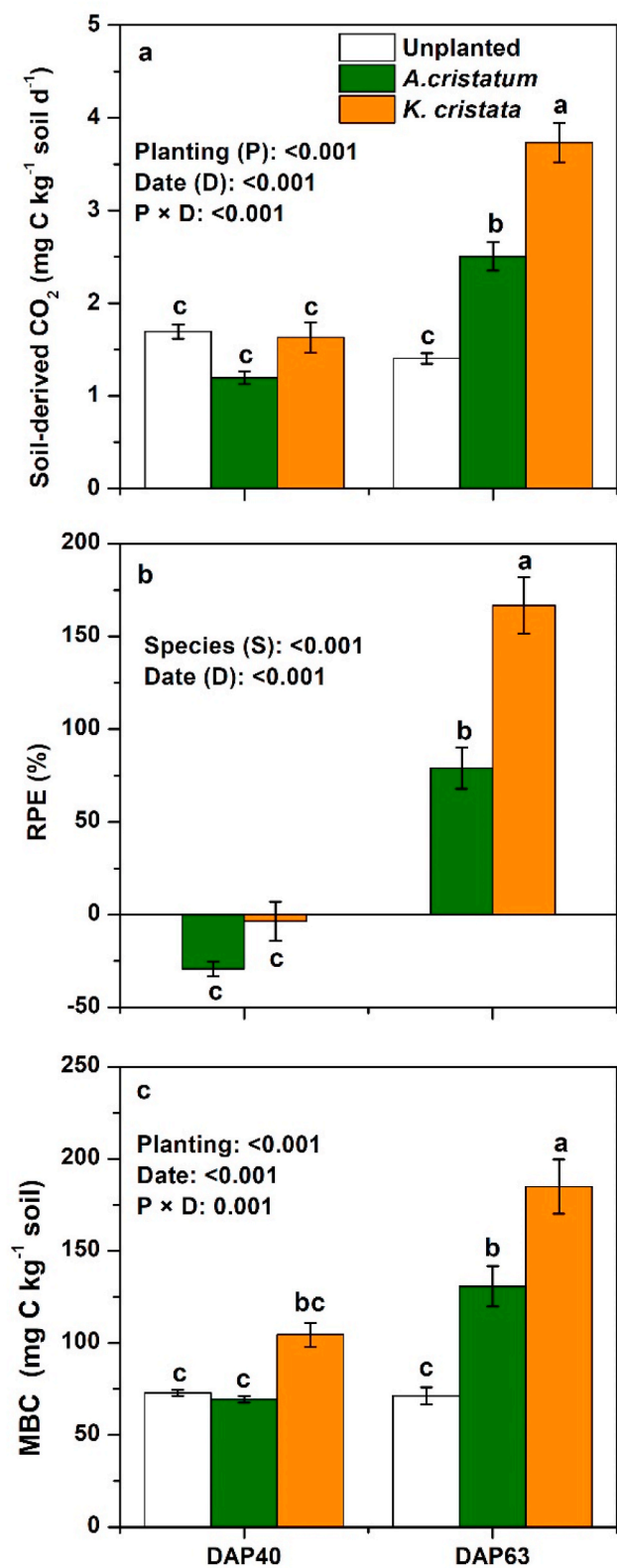
Fig. 4. Soil-derived CO_2 (a), rhizosphere priming effect (RPE, b) and microbial biomass C (MBC, c). Different lowercase letters indicate significant differences among treatments across the two sampling dates. Sub-legend shows ANOVA P-values. Date represents the sampling date. Error bars indicate the standard error of the mean; n = 4 for unplanted control and n = 5 for planted treatments except for the *A. cristatum* treatment at the second sampling date, where n = 3.

3.4. C concentrations and $\delta^{13}C$ values in bulk soil and aggregates

No significant differences in C concentrations and $\delta^{13}C$ values in bulk soil and each aggregate fraction were found between the unplanted control and planted treatments at each sampling date (Fig. 5). However, from DAP40 to DAP63, the $\delta^{13}C$ values of large- and small macroaggregates significantly decreased ($P < 0.001$; Fig. 5b), particularly the large macroaggregates in the planted treatments. Using the two-source model (details shown in the supplementary material), the amount of root-derived C entering the large macroaggregates was 0.34 and 0.33 (g C kg^{-1} large macroaggregates) for the *A. cristatum* and *K. cristata* treatments, respectively (Fig. S5).

4. Discussion

4.1. Variation in turnover rates of four aggregate fractions across two sampling dates

The potential importance of aggregate turnover in regulating SOC dynamic has been generally accepted, largely based on results of accessing static changes of overall soil aggregation or net changes of aggregate fractions (Yoo and Wander, 2008; Bach and Hofmockel, 2016). Our understanding of aggregate turnover rates including both formation and breakdown rates is still limited mainly due to methodological difficulties (De Gryze et al., 2006; Peng et al., 2017; Morris et al., 2019; Rahman et al., 2019). Using REOs labeling, we found that the turnover rates of aggregate fractions ranged from 0.006 to 0.024 day^{-1} (Fig. 3), *i.e.*, turnover time (the reciprocal of turnover rates) ranged from 41 to 168 days, which fall within the range reported by few empirical studies (Peng et al., 2017; Morris et al., 2019) and a modelling study (31–181 days; Segoli et al., 2013). Our results indicate that aggregate turnover rates may be dependent on aggregate size class. Compared to the other three aggregate fractions, microaggregates had relatively lower turnover rates (Fig. 3), which is broadly consistent with previous studies (De Gryze et al., 2006; Peng et al., 2017; Rahman et al., 2019) and suggests that microaggregates is relatively more stable and less sensitive to external disturbance (Tisdall and Oades, 1982; Six et al., 2000). The decreased aggregate turnover rates with sampling date, especially for larger aggregates (Fig. 3), indicate that aggregate stabilization may increase with time, which were also reported by previous studies (De Gryze et al., 2006; Peng et al., 2017).

By tracing REOs movements, to our best knowledge, our study is the first experimental study directly separating the breakdown from formation of soil aggregates in plant-soil systems. A few studies have investigated the effects caused by either root exudates or rhizosphere microorganisms on aggregate turnover (Peng et al., 2017; Morris et al., 2019), but without considering the effects of living roots. In our study, planting both decelerated and accelerated the breakdown and formation of different aggregate fractions depending on sampling date and species (Fig. S3; Table S2), although plant-induced formation of aggregates seemed to have the upper hand during plant growth of *K. cristata* (Fig. 2). Furthermore, these plant-induced changes in the transformation among aggregates led to distinct changes in the turnover rates of aggregates, *i.e.*, mostly decreases in large macroaggregates and increases in smaller aggregates (especially at DAP63, Fig. 3), broadly supporting our first hypothesis. These quantitative results on breakdown, formation and turnover of aggregates indicate that living roots have a much larger effect on soil aggregate dynamics than what we would have predicted based on traditional methods of measuring plant effects on net changes in soil aggregation (Haynes and Beare, 1997; Blankinship et al., 2016; Gould et al., 2016).

More importantly, *A. cristatum* and *K. cristata* caused significant differences in aggregate turnover (Figs. 2 and 3). We clearly found that *K. cristata* caused significantly greater increases in both aggregate breakdown and formation with plant growth, compared to *A. cristatum* (Fig. 2b and c). The specific root length, root length density and
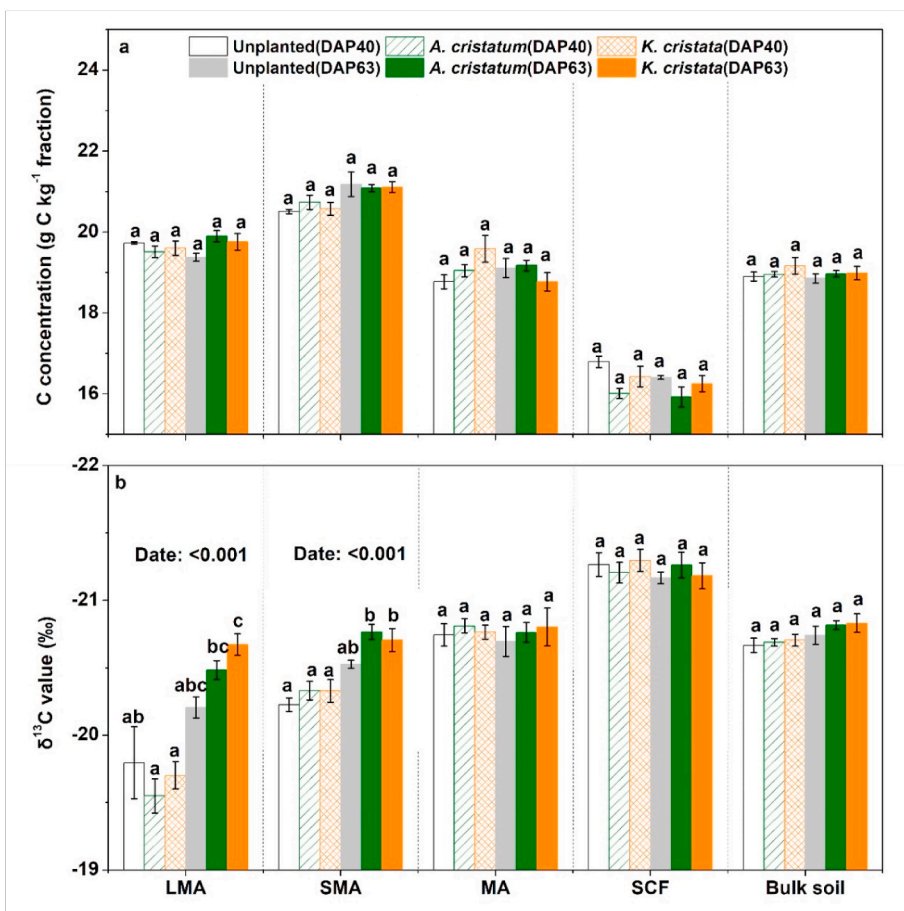
Fig. 5. C concentration (a) and δ¹³C value (b) in bulk soil and the four aggregate fractions. LMA, SMA, MA and SCF indicate the large macroaggregates, small macroaggregates, microaggregates and silt & clay fraction, respectively. Different lowercase letters indicate significant differences in the same fraction among treatments across the two sampling dates. Sub-legend shows ANOVA *P*-values. Date represents the sampling date. Error bars indicate the standard error of the mean; n = 4 for unplanted control and n = 5 for planted treatments except for the *A. cristatum* treatment at the second sampling date, where n = 3.
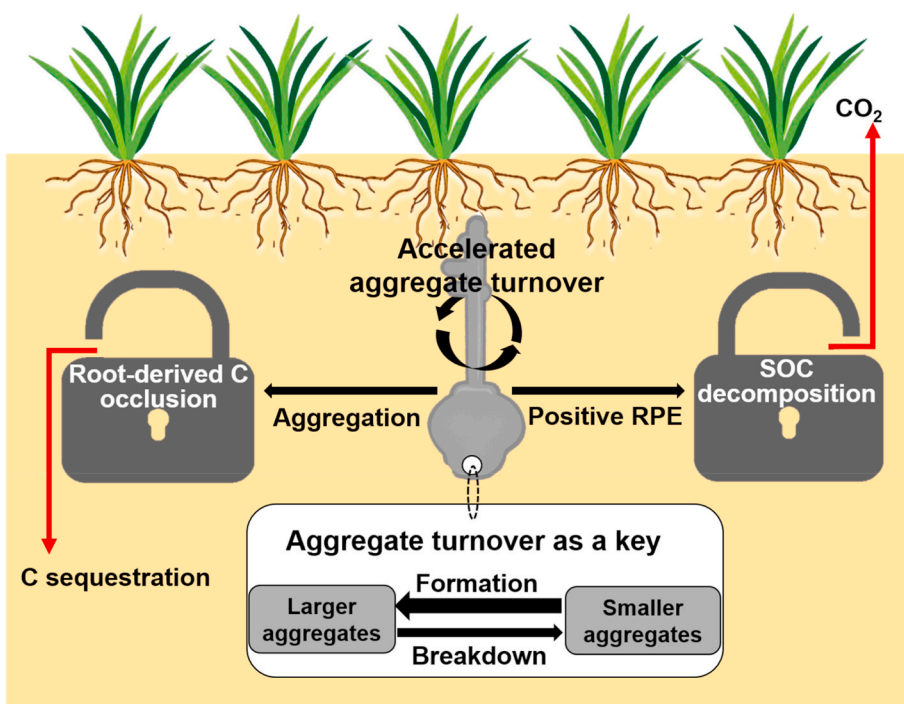
Fig. 6. A "key framework" depicting aggregate turnover regulating soil organic carbon (SOC) decomposition and sequestration. Presence of living roots accelerates aggregate turnover rates through enhancing both breakdown of existing aggregates and formation of new ones from smaller aggregates. The root-accelerated aggregate turnover increases the amount of microbial accessible substrates and then stimulates SOC decomposition by the enhanced rhizosphere priming effect (RPE). Concurrently, root-derived C is occluded inside the newly formed macroaggregates, which may be counteracted by C loss via the RPE. The thickness of arrows indicates the magnitude of processes or C fluxex. Further explanations are shown in the main text.

proportion of total root length attributed to <0.5 mm diameter roots were significantly higher for *K. cristata* than for *A. cristatum* (Table S3), suggesting that thinner roots, rather than root biomass and root-derived CO_2 (Fig. S4, a potential proxy of root exudates, Jones et al., 2009), may play an important role in regulating aggregate turnover through the penetration and entanglement (Rillig et al., 2015). These results suggest that more attention should be paid to the critical role of root traits in influencing aggregate turnover (Bardgett et al., 2014; Rillig et al., 2015; Poirier et al., 2018b).

4.2. The RPE was tightly associated with with root-driven aggregate turnover

Our study showed that plant growth and species significantly influenced the RPEs (Fig. 4b), consistent with others studies (Dijkstra et al., 2006; Yin et al., 2018; He et al., 2020). Here we argue that the species-specific differences in aggregate turnover contributed to the variation in the RPE between the two species. We found greater aggregate turnover rates for *K. cristata* than for *A. cristatum* at DAP63 (Fig. 3), indicating a greater release of previously aggregate-protected C, which could support the higher MBC and thereby causing the greater RPE for *K. cristata* (Fig. 4b and c). These findings suggest a tight association between root-driven aggregate turnover and the RPE. Recent studies confirmed the importance of root-induced changes in soil aggregation on the RPE (Lu et al., 2019; He et al., 2020; Wang et al., 2020). However, these recent studies were not able to determine aggregate turnover rates and thus may have underestimated or obscured the importance of aggregate turnover, particularly in cases where living roots either caused a lower than expected net breakdown of aggregates (He et al., 2020) or caused a significant net formation of aggregates (as shown in Fig. 1).

Tracing the species-specific variations in transformations among aggregates can further distinctly illuminate the role of aggregate breakdown, formation and turnover. On one hand, we found that the growth of *K. cristata* caused greater breakdown of large- and small macroaggregates (*i.e.* > 0.25 mm macroaggregates) than *A. cristatum* (Fig. 2b and c). Macroaggregates possess large amounts of highly bioavailable particulate organic matter (POM) (Six et al., 2000), and the release of POM after aggregate breakdown could further provide an energy and C source for microbial growth and extracellular enzyme production, thereby intensifying the positive RPE (Lu et al., 2019).

One the other hand, the species-specific variation in the transformations of microaggregates and silt & clay fraction (*i.e.* < 0.25 mm microaggregates) could also affect the RPE (Fig. 2b and c, and 4b). Microaggregates are mainly formed by mineral-organic complexation thereby physicochemically protecting SOC (Jastrow et al., 2007; Totsche et al., 2018). Root exudates (especially organic acids) adhering to the surface of microaggregates either can destabilize the mineral-organic complexation and liberate mineral-protected C via ligand exchange (Keiluweit et al., 2015; Jilling et al., 2018), or can directly activate microbes via alleviating microbial C limitation (Tian et al., 2016). The thinner roots of *K. cristata* than *A. cristatum* (Table S3) may have a greater ability of binding microaggregates and form macroaggregates after destabilizing the mineral-organic complexation of microaggregates. Thus, both increased breakdown and formation (*i.e.*, increased turnover) could have contributed to the greater RPE for *K. cristata* than for *A. cristatum* at the end of the experiment.

During the accelerated formation processes, root-derived C was preferentially sequestrated inside the newly formed macroaggregates, as indicated by the decreased δ^{13}C value in macroaggregates (especially large macroaggregates) in the planted treatments compared to the unplanted control at DAP63 (Fig. 5b). The higher amount of large macroaggregates (Fig. 1) but similar root-derived C concentration in this fraction (Fig. S5) for *K. cristata* than for *A. cristatum* indicated that more root-derived C was sequestrated in large macroaggregates for *K. cristata* (67 mg root-derived C kg^{-1} soil inside large macroaggregates *vs.* 31 mg

C kg^{-1} for *A. cristatum*). Similar results were observed in laboratory studies (Angers et al., 1997; Gale et al., 2000; Peng et al., 2017; Rahman et al., 2019). Further, the occluded root-derived C has the potential of being incorporated into microaggregates that form within macroaggregates over time (Gale et al., 2000), thereby becoming more stable (Totsche et al., 2018).

Therefore, despite the positive RPEs, we did not find a significant net C loss in our study (Fig. 5a). This finding is consistent with previous findings where the SOC loss caused by positive RPEs were counteracted by the sequestration of root-derived C via microbial biomass turnover (*i. e.*, Cheng, 2009 and Yin et al., 2019). Importantly, our finding provides an alternative mechanism (*i.e.*, aggregates physical protection) for the counteractive effect that roots have on SOC dynamics.

Our results supported our second hypothesis and for the first time provided direct evidence for the aggregate turnover hypothesis (Cheng et al., 2014), *i.e.*, by accelerating aggregate turnover, living roots can simultaneously increase the RPE and the sequestration of root-derived C. Hence, we here propose a new framework for SOC dynamics centered on root-driven aggregate turnover (Fig. 6): accelerated aggregate turnover by living roots acts as a "key" where aggregate breakdown may open the "lock" of SOC decomposition via the positive RPE, and simultaneously aggregate formation may open the other "lock" of turning root-derived C into occluded C causing C sequestration. The balance of the above two processes may determine the net change in SOC. This framework strongly emphasizes RPE as a crucial driver for SOC decomposition (Cheng et al., 2014; Finzi et al., 2015), and highly aligns with the emerging perspective that the soil structural matrix is a pivotal ecosystem property for protecting SOC (Schmidt et al., 2011; Six and Paustian, 2014).

4.3. Limitations and implications

Our study has some limitations. Firstly, we used small pots due to the difficulty in aggregate labeling with REOs (Peng et al., 2017) and wet-sieving, which may have limited the growing space and nutrient uptake by roots. However, we fertilized all the treatments with mineral N to relieve the potential N limitation. Secondly, although our results suggest that root-derived C could be occluded inside large macroaggregates, the natural ^{13}C labeling method did not allow us to accurately trace the accumulation of root-derived C within the time frame of our study. In the future, using a highly enriched ^{13}C labeling approach over a longer time period may provide more direct empirical evidence.

Our study and other recent studies (*e.g.* Lu et al., 2019; He et al., 2020; Wang et al., 2020) clearly indicate that living root-induced aggregate dynamics considerably influence the RPE and root-derived C sequestration (Fig. 6). Thus the regulation of aggregates on physical protection in plant-soil systems should receive more attention (Cheng et al., 2014). The new framework indicates that the potential changes in primary productivity and diversity, and associated changes in root traits, under global climate change scenarios are likely to affect the soil C cycle via altering aggregate turnover dynamics, which should merit greater consideration and be incorporated into biogeochemical models.

Declaration of competing interest

The authors declare that they have no known competing financial interests or personal relationships that could have appeared to influence the work reported in this paper.

Acknowledgements

Foundation of China (41601225, 31470625 and 31971635).

Appendix A. Supplementary data

Supplementary data to this article can be found online at https://doi.org/10.1016/j.soilbio.2020.107964.

References

Angers, D., Recous, S., Aita, C., 1997. Fate of carbon and nitrogen in water-stable aggregates during decomposition of $^{13}C^{15}N$-labelled wheat straw *in situ*. European Journal of Soil Science 48, 295–300.

Bach, E.M., Hofmockel, K.S., 2016. A time for every season: soil aggregate turnover stimulates decomposition and reduces carbon loss in grasslands managed for bioenergy. Global Change Biology Bioenergy 29, 588–599.

Bardgett, R.D., Mommer, L., De Vries, F.T., 2014. Going underground: root traits as drivers of ecosystem processes. Trends in Ecology & Evolution 29, 692–699.

Blankinship, J.C., Fonte, S.J., Six, J., Schimel, J.P., 2016. Plant versus microbial controls on soil aggregate stability in a seasonally dry ecosystem. Geoderma 272, 39–50.

Bond-Lamberty, B., Thomson, A., 2010. Temperature-associated increases in the global soil respiration record. Nature 464, 579–582.

Cheng, W., 2009. Rhizosphere priming effect: its functional relationships with microbial turnover, evapotranspiration, and C-N budgets. Soil Biology and Biochemistry 41, 1795–1801.

Cheng, W., Johnson, D.W., Fu, S., 2003. Rhizosphere effects on decomposition: controls of plant species, phenology, and fertilization. Soil Science Society of America Journal 67, 1418–1427.

Cheng, W., Kuzyakov, Y., 2005. Root effects on soil organic matter decomposition. In: Zobel, R.W., Wright, S.F. (Eds.), Roots and Soil Management: Interactions between Roots and the Soil, Agronomy Monograph No. 48. American Society of Agronomy, Crop Science Society of America, Soil Science Society of America, Madison, WI, USA, pp. 119–143.

Cheng, W., Parton, W.J., Gonzalez-Meler, M.A., Phillips, R., Asao, S., McNickle, G.G., Brzostek, E., Jastrow, J.D., 2014. Synthesis and modeling perspectives of rhizosphere priming. New Phytologist 201, 31–44.

Chivenge, P., Vanlauwe, B., Gentile, R., Six, J., 2011. Comparison of organic versus mineral resource effects on short-term aggregate carbon and nitrogen dynamics in a sandy soil versus a fine textured soil. Agriculture, Ecosystems & Environment 140, 361–371.

De Gryze, S., Six, J., Merckx, R., 2006. Quantifying water-stable soil aggregate turnover and its implication for soil organic matter dynamics in a model study. European Journal of Soil Science 57, 693–707.

Dijkstra, F., Cheng, W., Johnson, D., 2006. Plant biomass influences rhizosphere priming effects on soil organic matter decomposition in two differently managed soils. Soil Biology and Biochemistry 38, 2519–2526.

Elliott, E.T., 1986. Aggregate structure and carbon, nitrogen, and phosphorus in native and cultivated soils. Soil Science Society of America Journal 50, 627–633.

Finzi, A.C., Abramoff, R.Z., Spiller, K.S., Brzostek, E.R., Darby, B.A., Kramer, M.A., Phillips, R.P., 2015. Rhizosphere processes are quantitatively important components of terrestrial carbon and nutrient cycles. Global Change Biology 21, 2082–2094.

Gale, W., Cambardella, C., Bailey, T., 2000. Root-derived carbon and the formation and stabilization of aggregates. Soil Science Society of America Journal 64, 201–207.

Gentile, R., Vanlauwe, B., Six, J., 2011. Litter quality impacts short- but not long-term soil carbon dynamics in soil aggregate fractions. Ecological Applications 21, 695–703.

Gould, I.J., Quinton, J.N., Weigelt, A., De Deyn, G.B., Bardgett, R.D., Seabloom, E., 2016. Plant diversity and root traits benefit physical properties key to soil function in grasslands. Ecology Letters 19, 1140–1149.

Haynes, R.J., Beare, M.H., 1997. Influence of six crop species on aggregate stability and some labile organic matter fractions. Soil Biology and Biochemistry 29, 1647–1653.

He, Y., Cheng, W., Zhou, L., Shao, J., Liu, H., Zhou, H., Zhu, K., Zhou, X., 2020. Soil DOC release and aggregate disruption mediate rhizosphere priming effect on soil C decomposition. Soil Biology and Biochemistry 144, 107787.

Huo, C., Luo, Y., Cheng, W., 2017. Rhizosphere priming effect: a meta-analysis. Soil Biology and Biochemistry 111, 78–84.

Jastrow, J.D., Amonette, J.E., Bailey, V.L., 2007. Mechanisms controlling soil carbon turnover and their potential application for enhancing carbon sequestration. Climatic Change 80, 5–23.

Jilling, A., Keiluweit, M., Contosta, A.R., Frey, S., Schimel, J., Schnecker, J., Smith, R.G., Tiemann, L., Grandy, A.S., 2018. Minerals in the rhizosphere: overlooked mediators of soil nitrogen availability to plants and microbes. Biogeochemistry 139, 103–122.

Jones, D.L., Nguyen, C., Finlay, R.D., 2009. Carbon flow in the rhizosphere: carbon trading at the soil-root interface. Plant and Soil 321, 5–33.

Keiluweit, M., Bougoure, J.J., Nico, P.S., Pett-Ridge, J., Weber, P.K., Kleber, M., 2015. Mineral protection of soil carbon counteracted by root exudates. Nature Climate Change 5, 588–595.

Keith, A., Singh, B., Dijkstra, F.A., 2015. Biochar reduces the rhizosphere priming effect on soil organic carbon. Soil Biology and Biochemistry 88, 372–379.

Kuzyakov, Y., 2002. Review: factors affecting rhizosphere priming effects. Journal of Plant Nutrition and Soil Science 165, 382–396.

Lehmann, J., Kleber, M., 2015. The contentious nature of soil organic matter. Nature 528, 60–68.

Lu, J., Dijkstra, F.A., Wang, P., Cheng, W., 2019. Roots of non-woody perennials accelerated long-term soil organic matter decomposition through biological and physical mechanisms. Soil Biology and Biochemistry 134, 42–53.

Lützow, M.V., Kogel-Knaber, L., Ekschmitt, K., Matzner, E., Guggenberger, G., Marschner, B., Flessa, H., 2006. Stabilization of organic matter in temperate soils: mechanisms and their relevance under different soil conditions-a review. European Journal of Soil Science 57, 426–445.

Morris, E.K., Morris, D.J.P., Vogt, S., Gleber, S.C., Bigalke, M., Wilcke, W., Rillig, M.C., 2019. Visualizing the dynamics of soil aggregation as affected by arbuscular mycorrhizal fungi. The ISME Journal 13, 1639–1646.

Pausch, J., Loeppmann, S., Kühnel, A., Forbush, K., Kuzyakov, Y., Cheng, W., 2016. Rhizosphere priming of barely with and without root hairs. Soil Biology and Biochemistry 100, 74–82.

Peng, X., Zhu, Q., Zhang, Z., Hallett, P.D., 2017. Combined turnover of carbon and soil aggregates using rare earth oxides and isotopically labelled carbon as tracers. Soil Biology and Biochemistry 109, 81–94.

Plante, A.F., McGill, W.B., 2002. Soil aggregate dynamics and the retention of organic matter in laboratory-incubated soil with differing simulated tillage frequencies. Soil and Tillage Research 66, 79–92.

Poirier, V., Roumet, C., Angers, D.A., Munson, A.D., 2018a. Species and root traits impact macroaggregation in the rhizospheric soil of a Mediterranean common garden experiment. Plant and Soil 424, 289–302.

Poirier, V., Roumet, C., Munson, A.D., 2018b. The root of the matter: linking root traits and soil organic matter stabilization processes. Soil Biology and Biochemistry 120, 246–259.

Rahman, M.T., Liu, S., Guo, Z.C., Zhang, Z.B., Peng, X.H., 2019. Impacts of residue quality and N input on aggregate turnover using the combined ^{13}C natural abundance and rare earth oxides as tracers. Soil and Tillage Research 189, 110–122.

Rillig, M.C., Aguilar-Trigueros, C.A., Bergmann, J., Verbruggen, E., Veresoglou, S.D., Lehmann, A., 2015. Plant root and mycorrhizal fungal traits for understanding soil aggregation. New Phytologist 205, 1385–1388.

Schmidt, M.W., Torn, M.S., Abiven, S., Dittmar, T., Guggenberger, G., Janssens, I.A., Kleber, M., Kogel-Knabner, I., Lehmann, J., Manning, D.A., Nannipieri, P., Rasse, D.P., Weiner, S., Trumbore, S.E., 2011. Persistence of soil organic matter as an ecosystem property. Nature 478, 49–56.

Segoli, M., De Gryze, S., Dou, F., Lee, J., Post, W.M., Denef, K., Six, J., 2013. AggModel: a soil organic matter model with measurable pools for use in incubation studies. Ecological Modelling 263, 1–9.

Six, J., Bossuyt, H., De Gryze, S., Denef, K., 2004. A history of research on the link between (micro)aggregates, soil biota, and soil organic matter dynamics. Soil and Tillage Research 79, 7–31.

Six, J., Carpentier, A., Kessel, C.V., Merckx, R., Harris, D., Horwath, W.R., Lüscher, A., 2001. Impact of elevated CO_2 on soil organic matter dynamics as related to changes in aggregate turnover and residue quality. Plant and Soil 234, 27–36.

Six, J., Elliott, E.T., Paustian, K., 2000. Soil macroaggregate turnover and microaggregate formation: a mechanism for C sequestration under no-tillage agriculture. Soil Biology and Biochemistry 32, 2099–2103.

Six, J., Paustian, K., 2014. Aggregate-associated soil organic matter as an ecosystem property and a measurement tool. Soil Biology and Biochemistry 68, A4–A9.

Stamati, F.E., Nikolaidis, N.P., Banwart, S., Blum, W.E.H., 2013. A coupled carbon, aggregation, and structure turnover (CAST) model for topsoils. Geoderma 211–212, 51–64.

Tian, J., Pausch, J., Yu, G., Blagodatskaya, E., Kuzyakov, Y., 2016. Aggregate size and glucose level affect priming sources: a three-source-partitioning study. Soil Biology and Biochemistry 97, 199–210.

Tisdall, J.M., Oades, J.M., 1982. Organic matter and water-stable aggregates in soil. Journal of Soil Science 33, 141–163.

Totsche, K.U., Amelung, W., Gerzabek, M.H., Guggenberger, G., Klumpp, E., Knief, C., Lehndorff, E., Mikutta, R., Peth, S., Prechtel, A., Ray, N., Kogel-Knabner, I., 2018. Microaggregates in soils. Journal of Plant Nutrition and Soil Science 181, 104–136.

Vance, E., Brookes, P., Jenkinson, D., 1987. An extraction method for measuring soil microbial biomass C. Soil Biology and Biochemistry 19, 703–707.

Wang, X., Tang, C., Severi, J., Butterly, C.R., Baldock, J.A., 2016. Rhizosphere priming effect on soil organic carbon decomposition under plant species differing in soil acidification and root exudation. New Phytologist 211, 864–873.

Wang, X., Dijkstra, F.A., Yin, L., Sun, D., Cheng, W., 2020. Rhizosphere priming effects in soil aggregates with different size classes. Ecosphere 11, e03027.

Yang, S., Liu, W., Qiao, C., Wang, J., Deng, M., Zhang, B., Liu, L., 2019. The decline in plant biodiversity slows down soil carbon turnover under increasing nitrogen deposition in a temperate steppe. Functional Ecology 33, 1362–1372.

Yin, L., Corneo, P.E., Richter, A., Wang, P., Cheng, W., Dijkstra, F.A., 2019. Variation in rhizosphere priming and microbial growth and carbon use efficiency caused by wheat genotypes and temperatures. Soil Biology and Biochemistry 134, 54–61.

Yin, L., Dijkstra, F.A., Wang, P., Zhu, B., Cheng, W., 2018. Rhizosphere priming effects on soil carbon and nitrogen dynamics among tree species with and without intraspecific competition. New Phytologist 218, 1036–1048.

Yoo, G., Wander, M.M., 2008. Tillage effects on aggregate turnover and sequestration of particulate and humified soil organic carbon. Soil Science Society of America Journal 72, 670–676.

Zhang, X., Friedrich, J., Nearing, M.A., Norton, L., 2001. Potential use of rare earth oxides as tracers for soil erosion and aggregation studies. Soil Science Society of America Journal 65, 1508–1515.

Zhu, B., Gutknecht, J.L.M., Herman, D.J., Keck, D.C., Firestone, M.K., Cheng, W., 2014. Rhizosphere priming effects on soil carbon and nitrogen mineralization. Soil Biology and Biochemistry 76, 183–192.